ARC PRESSURE AND FLUID FLOW DURING ALTERNATING SHIELDING GASES – PART 2: ARC FORCE DETERMINATION

S.W. Campbell[1], A.M. Galloway[1] and N.A. McPherson[2]

[1]Department of Mechanical & Aerospace Engineering, University of Strathclyde, Glasgow
[2]BAE Systems Surface Ships Limited, 1048 Govan Road, Glasgow

Abstract

The transient variation of the shielding gas present in the alternating shielding gas process produces a dynamic action within the liquid weld metal. Flow vectors opposite in direction have been reported due to the various forces acting on the weld metal when argon and helium are present, however no data has been provided to substantiate this claim. This part of the study evaluates the various forces acting on the liquid weld metal when using argon and helium and their effects discussed.
It was determined that argon produces a greater vertically downward force in the central region than helium for both the arc force and Lorentz force. While helium produces a greater radially outwards force at the pool surface than argon due to plasma shear stress and Marangoni convection. In addition, the buoyancy force, i.e. the vertically upward force in the central portion of the weld metal, was greater for helium.

List of Symbols

P_{arc} Arc pressure (stagnation pressure at anode) (N/m^2),

ρ_g Density of the shielding gas (kg/m^3)

V Velocity (m/s)

μ_p Dynamic viscosity of the arc plasma (kg/(m.s))

I Current (A)

J Current density (A/m^2)

τ_p Plasma shear stress (N/m^2)

r Distance in the radial direction (m)

F_{arc} Arc force (N)

R Radius of arc (m)

F_L Lorentz force (N/m^3)

B Self-induced azimuthal magnetic field (N/(A.m))

μ_0 Permeability of free space (N/A^2)

F_B Buoyancy force

ρ_w Density of the weld metal (kg/m^3)

g Gravitational acceleration in negative z direction (m/s^2)

β Thermal expansion coefficient of the weld metal (1/K)

T Local reference temperature (K)

T_{ref} Arbitrary reference temperature (K) (melting temperature)

Ma Marangoni number (dimensionless)

$\frac{\delta\gamma}{\delta T}$ Temperature coefficient of surface tension (dyne/(cm.K))

ΔT Temperature difference between centre and edge of pool surface (K)

L Characteristic length (mm) (distance from weld centreline to fusion boundary)

μ_m Dynamic viscosity of the weld metal g/(cm.s)

α Thermal diffusivity (cm^2/s)

Introduction

The final weld geometry, in both gas tungsten arc welding (GTAW) and gas metal arc welding (GMAW), is influenced by the shielding gas used due to the unique arc characteristics each process generates. Fluid flow and heat flow are key factors in determining the final weld shape [1], with the direction of the liquid weld metal fluid flow being estimated based upon the various body forces acting upon it. The arc pressure distribution allows for the numerical derivation of various forces acting on the liquid weld metal including arc force, plasma shear and Lorentz force. In addition, the buoyancy force can also be determined numerically, whilst the surface tension gradient governs the Marangoni convection mode.

Alternating shielding gases is a relatively novel method of shielding gas delivery, and has been shown to produce a range of benefits including productivity [2-4], geometry [4,5], distortion reduction [2,3,6] and mechanical property improvements [2,3]. The process involves discretely supplying two different shielding gases (to date, argon or an argon based mixture and helium) in order to take advantage of the beneficial properties of each gas. The advantages generated previously have been based upon three independent phenomena [7]: a) variation in weld pool fluidity, b) arc pressure variation, and c) arc pressure peaking, that create fluid flow vectors opposite in direction for argon and helium [5].

Part 1 of this two part study discussed the effects that various welding parameters, i.e. welding current, shielding gas composition and pressure, tungsten electrode tip geometry, arc length and nozzle outlet diameter, have on the peak pressure and

pressure distribution within the arc column. As a result of the arc pressure distribution and other mechanical/material properties being a function of the shielding gas configuration, it can be inferred that the body forces acting upon the weld metal will also be affected. The measurements conducted show that there is a variation in arc pressure during the alternating shielding gas process but disproved the arc pressure peaking effect when both argon and helium are present whilst alternating from one gas to the other.

However, only limited data is available for the forces acting upon the liquid weld metal when using argon, with the equivalent data for helium being minimal. Thus, there is a requirement for data to validate the fluid flow assumptions in the alternating shielding gas process. Therefore, the aim of the present study is to evaluate the forces acting upon the liquid weld metal when using argon and helium, and describe the flow direction present when using each gas in order to more fully evaluate the flow regimes present when using alternating shielding gases.

Forces Acting on the Liquid Weld Metal

A schematic diagram of the GTAW process and the forces acting on the liquid weld metal are shown in Figure 1. As can be seen, the arc force and Lorentz force are opposite in direction to the plasma shear and buoyancy force, whilst the direction of flow due to Marangoni convection is dependent upon the surface tension gradient. Plasma shear is due to the arc plasma moving radially outwards on the weld pool surface, causing a drag force, and is therefore a function of the dynamic viscosity and radial velocity of the shielding gas. Lee and Na [10] used numerical modelling to simulate the GTAW process and presented results for the plasma shear over a range of welding currents and electrode vertex angles. They determined that a maximum

shear force occurred between 1 and 2 mm from the arc centreline, which for a 60° vertex angle they found to be approximately 15, 75 and 155 N/m^2 for a 100, 200 and 300 A welding current respectively. Hu and Tsai [11] also used numerical modelling to simulate a GMAW arc and found that a plasma shear of approximately 90 N/m^2 was produced for a welding current of 220 A.

The arc force is defined as the force of the arc plasma impinging upon the weld pool surface for which there are several methods of determining; experimentally measure the arc force using a torsion bar and displacement transducer [8], or numerically integrate the arc pressure over the impingement area of the arc [9]. Lin and Eagar [9] presented arc force data for a range of welding currents and electrode vertex angles whilst using argon, showing that the arc force is proportional to the square of the current.

The Lorentz (or electromagnetic) force is one of the driving forces for fluid flow in the weld pool [12-15]. Kou and Wang [12] demonstrated using 3D mathematical modelling, and by considering various driving forces individually (electromagnetic, buoyancy and surface tension), that the electromagnetic force produced deeper penetration than those attributed to the buoyancy force or surface tension effects. Computational simulations generally include the effect of buoyancy and surface tension on the weld metal, however, modelling only has only been used to simulate the driving forces individually or as part of a combination of driving forces, and the effect of the shielding gas has never been considered. Kou and Sun [13] demonstrated experimentally using alternative heat sources that the buoyancy force produced shallower penetration in the central location but was radially wider than the Lorentz force.

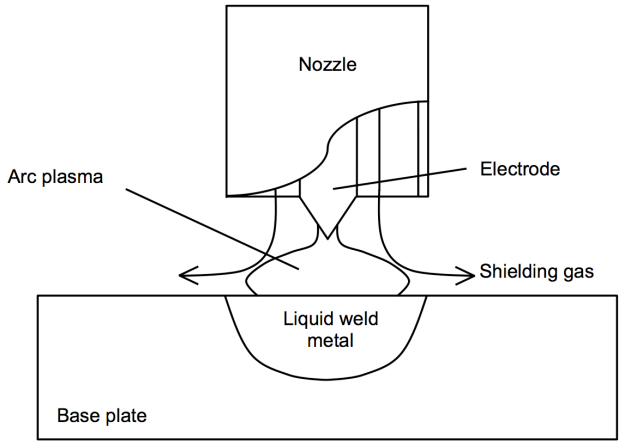

(a)

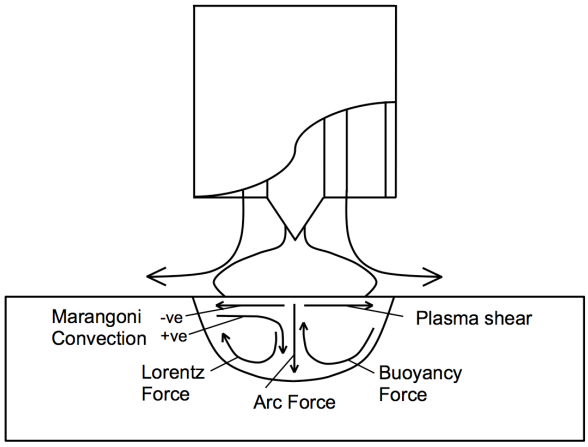

(b)

Figure 1: Schematic diagram of (a) GTAW process and (b) Forces acting on liquid weld metal

Experimental Setup

The forces acting on the liquid weld metal are derived from the arc pressure measurements generated in Part 1 of this research.

Subsequent trials for the measurement of weld geometry were conducted on an automated welding rig, which moved the plate beneath a stationary welding torch. Trials were performed on 250 x 100 x 6 mm thick DH36 grade steel, with the travel speed being altered to maintain a constant power input due to the varying arc voltage; a variation of less than 1% was achieved whilst assuming a constant thermal

efficiency of unity. The weld parameters for this element of investigation are shown in Table 1.

Shielding Gas Configuration	Arc Length (mm)	Current (A)	Voltage (V)	Travel Speed (mm/s)	Heat Input (J/mm)
Argon	2	200	14.2	3.7	767.6
Helium	2	200	19.2	5.0	768.0
Alternating Shielding Gases	2	200	16.8	4.4	763.6
GTAW-P	2	200 (peak) 100 (background)	14.2	2.8	760.7

Table 1: Weld parameters for bead on plate trials

Results and Discussion

Figure 2 shows the radial pressure distribution with respect to the arc centreline for argon and helium shielding gases generated in Part 1 of this research. The arc pressure distribution allows for the derivation of other important plasma aspects including the plasma shear force, arc force, and Lorentz force.

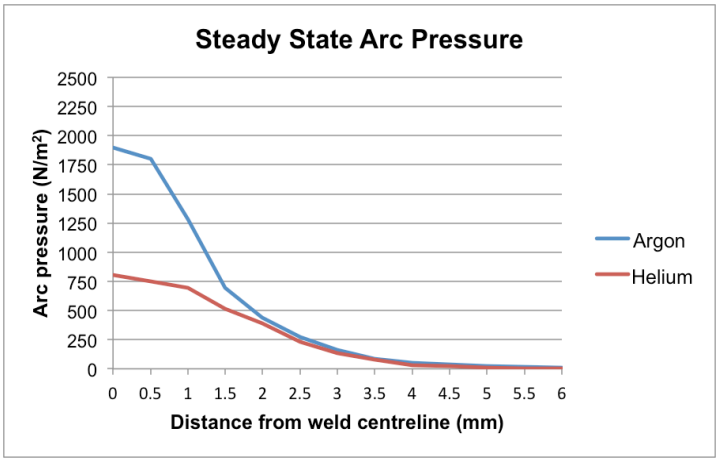

Figure 2: Steady-state arc pressure

Since the pressure reported is essentially the stagnation pressure of the plasma jet arrested at the anode plate surface, the velocity of the plasma jet can be determined using Bernoulli's theorem, equation (1). While Lin and Eager [9] reported that

equation (2), derived by Maecker based upon Bernoulli's theorem, was the most consistent with their experimental data.

$$P_{arc} = \frac{1}{2}\rho_g v^2 \tag{1}$$

$$v = \sqrt{\frac{\mu_p IJ}{2\pi\rho_g}} \tag{2}$$

Figure 3 shows the axial velocity distribution of the arc plasma at the plate surface. The shielding gas densities (0.05 kg/m^3 for argon and 0.01 kg/m^3 for helium) and dynamic viscosities (both approximately 2.75x10^{-4} kg/ms) were taken from graphs presented by Traida et al. [16] based on a temperature of the plasma of 10000 K adjacent to the plate surface [17]. The axial velocity of the helium plasma is considerably higher than that of argon, primarily due to the respective densities of the shielding gases.

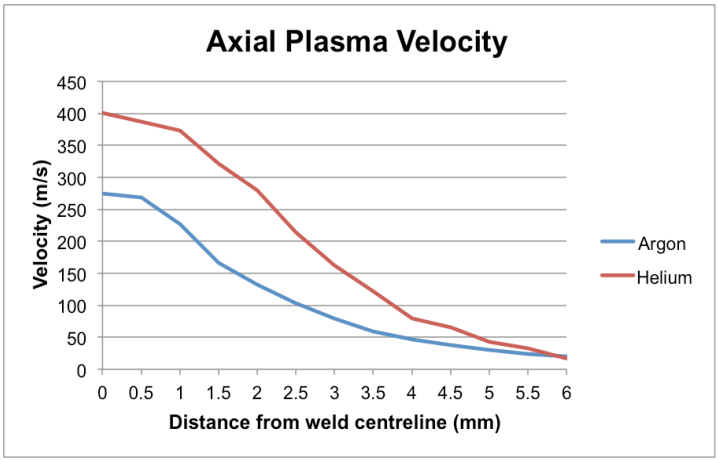

Figure 3: Steady-state plasma velocity

The plasma shear stress can be calculated using equation (3). The plasma shear stress causes the liquid weld metal to flow from the centre of the pool surface towards the pool boundary and return beneath the pool surface.

$$\tau_p = \mu_p \frac{\delta v}{\delta r} \tag{3}$$

The plasma shear stress distribution on the plate surface is shown in Figure 4. As can be seen, the peak shear stress occurs away from the weld centreline, this is because the plasma shear stress is a function of the gradient of the radial velocity. The maximum shear stress for argon (~80 N/m^2) was found to be 1 mm from the weld centreline, which was in agreement with Lee and Na [10] and Hu and Tsai [11] who reported values of ~75 N/m^2 and ~90 N/m^2 respectively at a distance approximately 1 mm from the weld centreline for argon.

As can be seen in Figure 4, the maximum shear stress generated when using helium (~240 N/m^2) was approximately three times greater than that of argon. This implies that the liquid weld metal is more likely to flow radially outwards at the pool surface when using helium than argon.

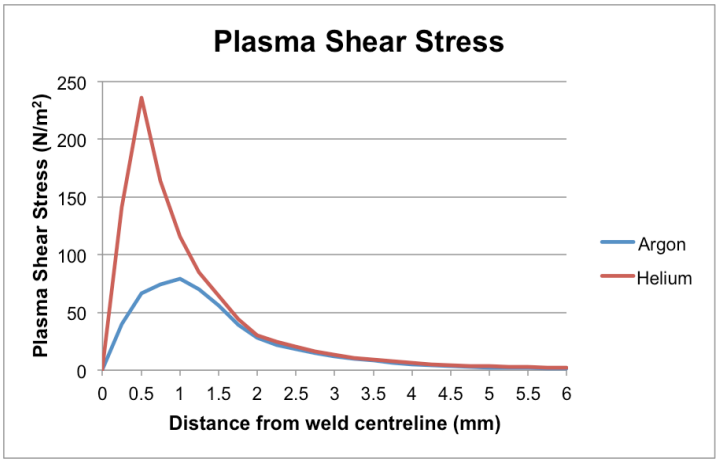

Figure 4: Plasma shear stress distribution

The arc force can be determined by integrating the arc pressure distribution over the area of the arc:

$$F_{arc} = \int_0^R 2\pi r P_{arc}\, dr \qquad (4)$$

A diameter of 7.5 mm and 6.5 mm for argon and helium respectively was measured using image analysis software in Part 1. This allowed for the arc force over the effective area of the arc to be determined; an arc force of ~1800 dyne and ~1140

dyne was calculated for argon and helium respectively. The arc force for argon is in good agreement with the experimental parabolic arc force relationship with current that Lin and Eagar [9] reported for argon. The arc force distribution, Figure 5, was determined by numerical integration being performed over 0.0625 mm segments using equation (4), and, as shown, the peak arc force occurs approximately 1-2 mm from the weld centreline.

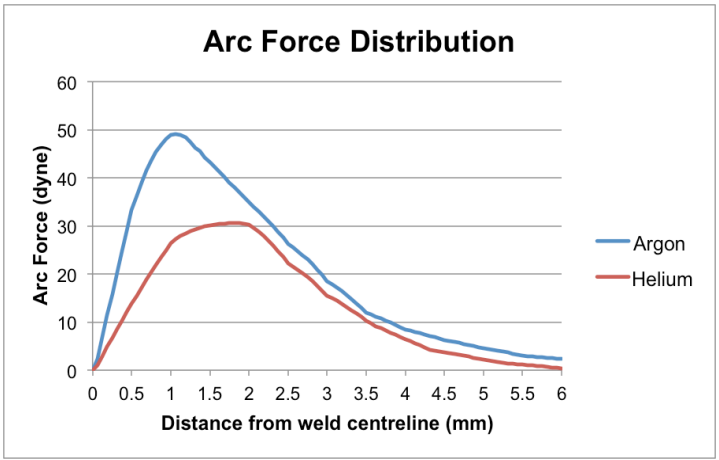

Figure 5: Arc force distribution

The Lorentz force can be calculated using:

$$F_L = JB \tag{5}$$

Where J, the current density, and B, the self-induced azimuthal magnetic field, can be derived using equation (6) and Ampere's equation (equation (7)) respectively:

$$J = \frac{P_{arc} I}{F_{arc}} \tag{6}$$

$$B = \frac{\mu_0}{r} \int_0^R Jr\, dr \tag{7}$$

Combining equation (6) and (7) yields:

$$B = \frac{\mu_0 I}{2\pi r} \tag{8}$$

The Lorentz force distribution is shown in Figure 6, as with the arc force distribution, calculations have been performed over 0.0625 mm segments. As can be seen, at the arc centreline the Lorentz force is zero, this is because the integration constant B term (equation (7)) tends to zero when r tends to zero. Moving radially outwards, <1.25 mm, argon produced a Lorentz force approximately double that of helium. However, helium produced a higher Lorentz force >1.25 mm to the edge of the arc. Summating the results over the arc area produced a total Lorentz force of $5.08*10^5$ N/m^3 for argon and $3.25*10^5$ N/m^3 for helium.

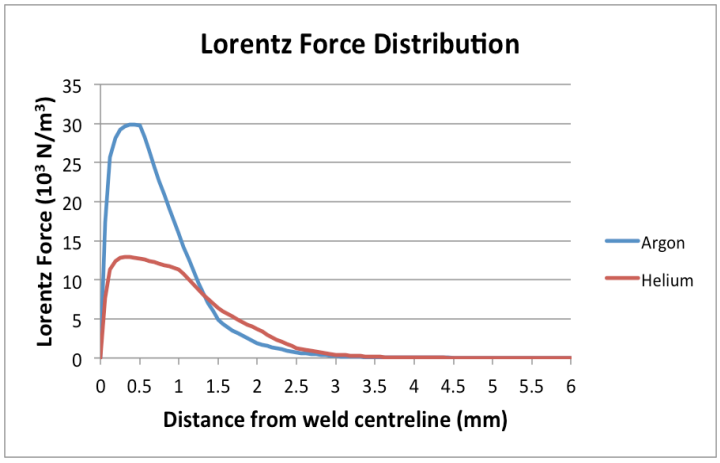

Figure 6: Lorentz force distribution

The buoyancy force can be calculated using the Boussinesq approximation:

$$F_B = -\rho_w g \beta (T - T_{ref}) \tag{9}$$

Recently, linear thermal expansion data for the weld metal produced for different shielding gases has been produced for temperatures up to 1200°C (1473K) [18]. It was found that the weld metal produced using an argon/CO_2 shielding gas mixture has a higher coefficient of thermal expansion than helium. However, the maximum difference in thermal expansion between shielding gases, approximately 0.6 x 10^{-6} /K, equates to only 4.6%, and can be considered negligible in comparison to the $(T - T_{ref})$ term, when considering a peak temperature in the weld pool of

approximately 2350K and 3700K for argon and helium respectively [19]. This results in helium having a $(T - T_{ref})$ term in excess of three times that of argon and, by assuming that the other terms are negligible, helium would have a buoyancy force approximately three times greater than argon.

The surface tension (or Marangoni convection mode) is generally discussed as a function of the surface-active elements, such as sulphur or oxygen [20,21]. The surface tension gradient is also a function of temperature; a negative surface tension gradient acts to pull the weld metal outwards and, conversely, a positive surface tension gradient acts to pull the weld metal inwards. Limmaneevichitr and Kou [22] simulated the fluid flow due to Marangoni convection in a transparent $NaNO_3$ solution using a laser power source for a range of power inputs and laser diameters. They found that a high beam power input produced faster, shallower convection than a low beam power input. In addition, they demonstrated that a small beam diameter produced faster, deeper convection than a larger beam diameter.

Due to the unique characteristics, helium produces a greater voltage potential than argon; in this study 19.2 V and 14.2 V respectively, and therefore a power input 35% greater than argon (assuming that the thermal efficiency is constant). The impingement diameter of the welding arc was also found to change depending on the shielding gas used; as discussed previously, argon and helium produced an effective arc diameter of 7.5 and 6.5 mm respectively. Therefore, based on the findings of Limmaneevichitr and Kou [22], helium would produce faster convection than argon.

The Marangoni number has been widely used for the measure of the extent of Marangoni convection and is given by equation (10):

$$Ma = \frac{-\frac{\delta\gamma}{\delta T}(\Delta T)L}{\mu_m \alpha} \tag{10}$$

Using values previously published for steel of negligible sulphur content, $-\frac{\delta\gamma}{\delta T}$, μ_m and α, of -0.3 dyne/(cm.K), 5 x 10^{-2} g/(cm.s) and 5 x 10^{-2} cm^2/s respectively [22], ΔT of 650 K and 2000 K for argon and helium respectively [19] and a characteristic length L of 4.4 mm and 4.8 mm for argon and helium respectively as determined by this study, the Marangoni number can be determined. Therefore, since the temperature coefficient of surface tension is negative, the flow is radially outwards on the pool surface and a Marangoni number of 3.43 x 10^4 for argon and 1.15 x 10^5 for helium calculated; this implies that the flow becomes stronger [23], i.e. the flow velocity increases. The Marangoni number for argon is in line with those presented elsewhere [22].

Macrographs of the weld geometry produced with constant heat input using the various shielding gas and power input methods are shown in Figure 7. As can be seen, the weld produced using helium resulted in a considerably wider weld bead (~9.6 mm) compared to argon (~8.8 mm), whilst alternating shielding gases (~9.2 mm) was in between and GTAW-P was narrower (~8.2 mm) due to the fluidity of the weld pool during the background current phase. However, the maximum penetration in the centre of the weld were fairly similar (3-3.2 mm). Thus there is considerably more variation in the weld width than the penetration depth, indicating that the plasma shear stress, buoyancy force and Marangoni convection have a greater influence on the solidified weld geometry than the arc force and Lorentz force.

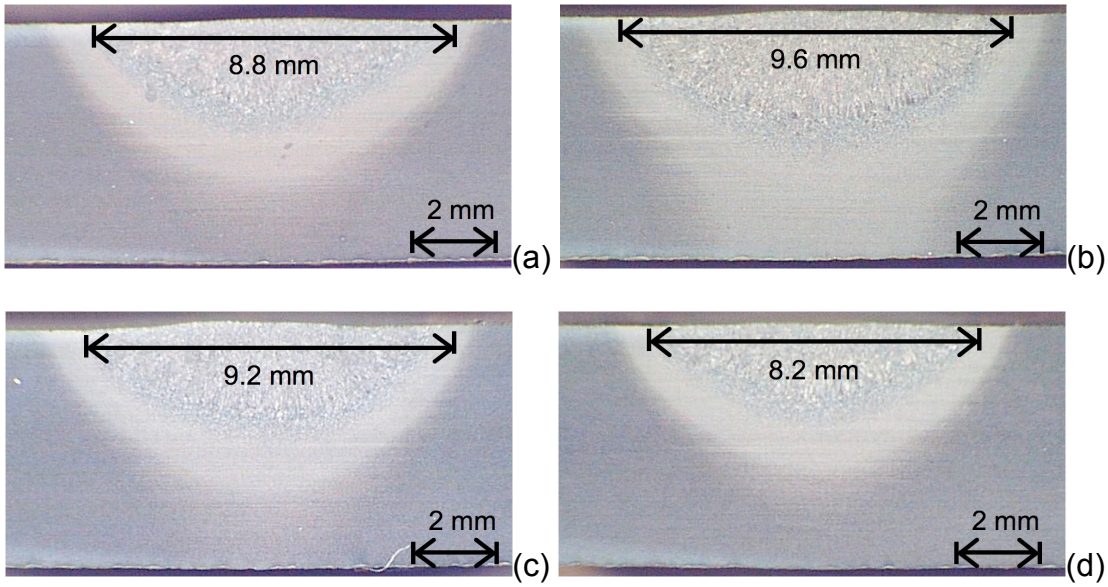

Figure 7: Weld macrograph for (a) Argon, (b) Helium, (c) Alternating shielding gases, and (d) GTAW-P

Conclusions

A comparison of the forces acting upon the liquid weld metals has been conducted for argon and helium shielding gases. The results can be summarised as follows:

- Helium produces a greater plasma shear stress than argon. The maximum shear stress occurs approximately 1 mm from the weld centreline, and is approximately 80 N/m^2 and 240 N/m^2 for argon and helium respectively.
- Argon produces a greater arc force both in the central location and over the effective area of the arc (~1800 dyne and ~1140 dyne, for argon and helium respectively).
- Argon also produces a greater Lorentz force than helium, $5.08*10^5$ N/m^3 and $3.25*10^5$ N/m^3 respectively. The Lorentz force distribution showed that argon had a considerably greater core (<1.25 mm radius) Lorentz force, whilst helium produced a greater Lorentz force outwith the core (1.25 mm to arc edge).

- The buoyancy force was estimated to be approximately three times greater for helium than argon due to the higher maximum temperature in the weld pool.
- The Marangoni convection was estimated based on results from this study and previously published data. It was found that using helium resulted in a greater Marangoni number 1.15×10^5 than argon 3.43×10^4, indicating that the flow became stronger and the outwards flow velocity increased.

As a result of the forces acting on the liquid weld metal, it can be inferred that the flow vectors for helium are opposite in direction to those produced to that using argon. This therefore implies that the resulting flow vectors during alternating shielding gases will fluctuate from one flow direction to the other; creating a dynamic effect within the liquid weld metal.

This dynamic effect would not be present in GTAW-P, as the flow would all be in the direction produced by argon. However, the magnitude of the forces would fluctuate when switching between the peak and background current, creating a ‘jerking’ effect on the liquid weld metal.

Acknowledgements

The authors would like to acknowledge the funding provided by BAE Systems Surface Ships Limited, which has made this research possible.

References

1. M.H. Cho, Y.C. Lim and D.F. Farson: ‘Simulation of weld pool dynamics in the stationary pulsed gas metal arc welding process and final weld shape’, Welding Journal, 2006, **85(12)**, 271-283.

2. S.W. Campbell, A.M. Galloway and N.A. McPherson: ‘Techno-economic evaluation on the effects of alternating shielding gases for advanced joining processes’, Proceedings of the Institution of Mechanical Engineers, Part B: Journal of Engineering Manufacture, 2011, **225(10)**, 1863-1872.
3. S.W. Campbell, A.M. Galloway and N.A. McPherson: ‘Evaluation of gas metal arc welding with alternating shielding gases for use on AA6082T6’, Proceedings of the Institution of Mechanical Engineers, Part B: Journal of Engineering Manufacture, 2012, **226(6)**, 992-1000.
4. S.W. Campbell, A.M. Galloway and N.A. McPherson: ‘Artificial neural network prediction of weld geometry performed using GMAW with alternating shielding gases’, Welding Journal, 2012, **91(6)**, 174s-181s.
5. B.Y. Kang, Y.K.D.V. Prasad, M.J. Kang, K.J. Kim and I.S. Kim: ‘Characteristics of alternate supply of shielding gases in aluminium GMA welding’, Journal of Materials Processing Technology, 2009, **209(2009)**, 4716-4721.
6. B.Y. Kang, Y.K.D.V. Prasad, M.J. Kang, K.J. Kim and I.S. Kim: ‘The effect of alternate supply of shielding gases in austenite stainless steel GTA welding’, Journal of Materials Processing Technology, 2009, **209(2009)**, 4722-4727.
7. Y.H. Chang: ‘Improve GMAW and GTAW with alternating shielding gases’, Welding Journal, 2006, **85(2)**, 41-43.
8. T.D. Burleigh and T.W. Eagar: ‘Measurement of the force exerted by a welding arc’, Metallurgical Transactions A, 1982, **14A**, 1223-1224.
9. M.L. Lin and T.W. Eagar: ‘Pressures produced by gas tungsten arcs’, Metallurgical Transactions B, 1986, **17B**, 601-607.

10. S.Y. Lee and S.J. Na: ‘Analysis of TIG welding arc using boundary-fitted coordinates’, Proceedings of the Institution of Mechanical Engineers, Part B: Journal of Engineering Manufacture, 1995, **209(2)**, 153-164.
11. J. Hu and H.L. Tsai: ‘Heat and mass transfer in gas metal arc welding. Part 1: The arc’, International Journal of Heat and Mass Transfer, 2007, **50(2007)**, 833-846.
12. S. Kou and Y.H. Wang: ‘Weld pool convection and its effect’, Welding Journal, 1986, **65(3)**, 63-70.
13. S. Kou and D.K. Sun: ‘Fluid flow and weld penetration in stationary arc welds’, Metallurgical Transactions A, 1985, **16A**, 203-213.
14. G.M. Oreper, T.W. Eagar and J. Szekely: ‘Convection in arc weld pools’, Welding Journal, 1983, **62(11)**, 307-312.
15. A. Matsunawa, S. Yokoya and Y. Asako: ‘Convection in weld pool and its effect on penetration shape in stationary arcs’, Transactions of JWRI, 1987, **16(2)**, 229-236.
16. A. Traidia, F. Roger, A. Chidley, J. Shroeder and T. Marlaud: ‘Effect of helium-argon mixtures on the heat and fluid flow in gas tungsten arc welding’, World Academy of Science, Engineering and Technology, 2011, **49**, 1053-1058.
17. F. Lago, J.J. Gonzalez, P. Freton and A. Gleizes: ‘A numerical modelling of an electric arc and its interaction with the anode: Part 1. The two-dimensional model’, Journal of Physics D: Applied Physics, 2004, **37(2004)**, 883-897.
18. F.H. Ley, S.W. Campbell, A.M. Galloway and N.A. McPherson: unpublished work, 2013.

19. A. Traidia and F. Roger: ‘A computational investigation of different helium supplying methods for the improvement of GTA welding’, Journal of Materials Processing Technology, 2011, **211(2011)**, 1553-1562.
20. K.C. Mills, B.J. Keene, R.F. Brooks and A. Shirali: ‘Marangoni effects in welding’, Philosophical Transactions of the Royal Society A, 1998, **356**, 911-925.
21. D.K. Aidun and S.A. Martin: ‘Effect of sulphur and oxygen on weld penetration of high-purity austenitic stainless steel’, Journal of Materials Engineering and Performance, 1997, **6(4)**, 496-502.
22. C. Limmaneevichitr and S. Kou: ‘Visualization of Marangoni convection in simulated weld pools’, Welding Journal, 2000, **79(5)**, 126-135.
23. S. Kou, C. Limmaneevichitr and P.S. Wei: ‘Oscillatory Marangoni flow: a fundamental study by conduction-mode laser spot welding’, Welding Journal, 2011, **90(12)**, 229-240.